# Iron oxide-mediated photo-Fenton catalysis in the inactivation of enteric bacteria present in wastewater effluents at neutral pH

Fernández, L.[1], González-Rodríguez, J.[1]*, Gamallo, M.[1], Vargas-Osorio, Z.[2,3], Vázquez-Vázquez, C.[2], Piñeiro, Y.[2], Rivas, J.[2], Feijoo, G.[1], Moreira, M.T.[1]

[1] CRETUS Institute. Department of Chemical Engineering. Universidade de Santiago de Compostela, 15782 Santiago de Compostela, Spain.

[2] Laboratory of Magnetism and Nanotechnology. Departments of Physical Chemistry, Faculty of Chemistry, and Applied Physics, Faculty of Physics. Universidade de Santiago de Compostela, 15782, Santiago de Compostela, Spain.

[3] Department of Biomaterials, Centre for Functional and Surface Functionalized Glass (FUNGLASS), Alexander Dubcek University of Trencin, Slovakia.

* Corresponding author: jorgegonzalez.rodriguez@usc.gal; Tel.: +34-8818-16771

**Abstract:** The pressure on natural water resources associated with increasing water scarcity highlights the value of using reclaimed water through the development of efficient and environmentally friendly treatment technologies. In this work, the use of magnetic nanoparticles in photo-Fenton catalysis for water disinfection was considered to inactivate natural enteric bacteria present in municipal wastewater effluents under white light and neutral pH. The most recommended ranges were evaluated in key variables such as the loading and composition of nanoparticles (NPs), hydrogen peroxide ($H_2O_2$) concentration, the light source (UV and visible) and treatment time were evaluated in wastewater disinfection expressed in terms of total coliforms and *Escherichia coli* colony forming units (CFU). The magnetic separation of NPs allowed the disinfection process to be carried out in different cycles, facilitating the recovery of the nanocatalyst and avoiding its discharge with the treated effluent.

**Keywords:** disinfection, wastewater, photo-Fenton, magnetic nanoparticles, SBA15

# Introduction

In wastewater treatment plants (WWTP) several physical and chemical transformations are carried out to ensure the environmental safety of the treated effluent before its discharge into the natural environment. In this field, the regulatory framework established by the European Council Directive 91/271/EEC on wastewater treatment (European Union, 1991) defined the quality standards of the effluents treated before their discharge into the environment and the processes required to achieve these objectives. However, in most cases these conventional processes do not always guarantee the removal of certain toxic compounds, pathogens or viruses in the effluent, posing a risk not only to the environment but also to human health (García-Fernández et al., 2019; Mirzaei et al., 2017). For this reason, the development of advanced treatments capable of removing these compounds and microorganisms is necessary to ensure the safety of the effluents. Actually, for disinfection purposes, the most widely used alternative is UV treatment, but the high energy requirements of this technology limit the viability of its operation and maintenance (Rodriguez-Narvaez et al., 2017).

Therefore, improving effluent quality for reuse is an important factor to consider for the design of treatment plants (Purnell et al., 2020), especially since the reuse of wastewater could be one of the largest water resources if the reclaimed water quality standards are achieved (Chong et al., 2010). In line with this, one of the sustainable development objectives related to water scarcity is addressed: access to drinking water (Sgroi et al., 2018). Depending on the physicochemical and microbiological parameters of water quality, there are different applications for reclaimed water, such as urban, agricultural, industrial, recreational and environmental restoration. However in all cases it is necessary to reduce the risk factors associated not only with emerging micropollutants or heavy metals, but also with the presence of bacteria, viruses or parasites in the treated effluents before their use (Shannon et al., 2008). The most widely considered option is to discharge the effluent into an environmental buffer (i.e. river, aquifer, lake, ...), considering that the pollutant load is diluted in the environment and the risks associated with the use of this water are reduced. In this framework, several reference bodies such as the World Health Organization (World Health Organization, 2006) or US Environmental Protection Agency (US Environmental Protection Agency, 2012) have published guidelines for the reuse of water on a case-by-case basis that provide clear guidance in this field.

Within wastewater facilities, the disinfection of the treated effluent before its discharge relies on Advanced Oxidation Processes (AOPs), mainly UV light and/or ozone treatment. The generation of reactive oxygen species (ROS) that takes place in these processes allows the inactivation of bacteria, viruses, fungi or algae. Furthermore, other AOP processes are based on the use of semiconductors such as $TiO_2$ or ZnO materials (Mirzaei et al., 2016; Pigeot-Rémy et al., 2011) and Fenton catalysts, either in free form (González-Rodríguez et al., 2020) or immobilized onto supports (membranes or granular activated carbon) (Ferreiro et al., 2019). In this area, two different ways are investigated: homogeneous and heterogeneous catalysis. The main disadvantage of homogeneous catalysis processes is the impossibility of retaining the catalyst in the system, so efficient separation is required to prevent further water pollution (Bautista et al., 2008), but the reaction kinetics is not subjected to mass transfer limitation between the different phases. In addition, in the case of Fenton catalysis, strict control of the pH is required, because the iron salts precipitate at pH values above 3, forming hydroxides and radically decreasing the reaction rates. Specific trends in this field of research are to promote the formation of iron complexes by adding other chemical compounds as ethylenediamine-N,N'-disuccinic acid (EDDS), citrate or oxalate (Miralles-Cuevas et al., 2014; Mirzaei et al., 2017). As

an improvement strategy, the use of iron nanoparticles with magnetic properties in heterogeneous catalysis is proposed so that they are recovered when an external magnetic field is applied. These magnetic nanoparticles can be coated by polymers or supported by other matrices (i.e. carbon- or silica-based structures or zeolites) to improve stability and prevent agglomeration (Mirzaei et al., 2017). This option would not only avoid the discharge of iron ions into the treated effluent but also the use of stabilizing agents for complex formation. There are not all advantages in heterogeneous catalysis, lower reaction rates are observed in heterogeneous processes mainly due to limitations in mass transfer, which would imply a higher demand for catalyst loading.

One option that combines the advantages of photocatalysis and the Fenton reaction is based on the photo-Fenton process, a system that has proven effective in the degradation of contaminants (Davididou et al., 2019; Fernández et al., 2019) and inactivation of microorganisms (Baniamerian et al., 2018; Giannakis et al., 2016) (Figure 1). Firstly, the adsorption of the microorganisms onto the surface of the catalyst takes place due to the electrostatic interactions between them. This surface charge in the case of nanoparticles is a function of the pH value and the composition of the catalyst surface (i.e. coated-NP or immobilized NP on supports) and for the microorganisms, the composition and characteristics of the membrane play an important role together also with the pH. In this system, the generation of ROS during irradiation causes the oxidation/reduction of phospholipids and the leakage of ions, destabilizing the membrane. Once the membrane is broken, the interaction of the ROS with the cell components affects the metabolic pathways of the microorganisms and in the specific case of viruses, oxidation of the protein cover is mainly responsible for the inactivation mechanism (Laxma Reddy et al., 2017).

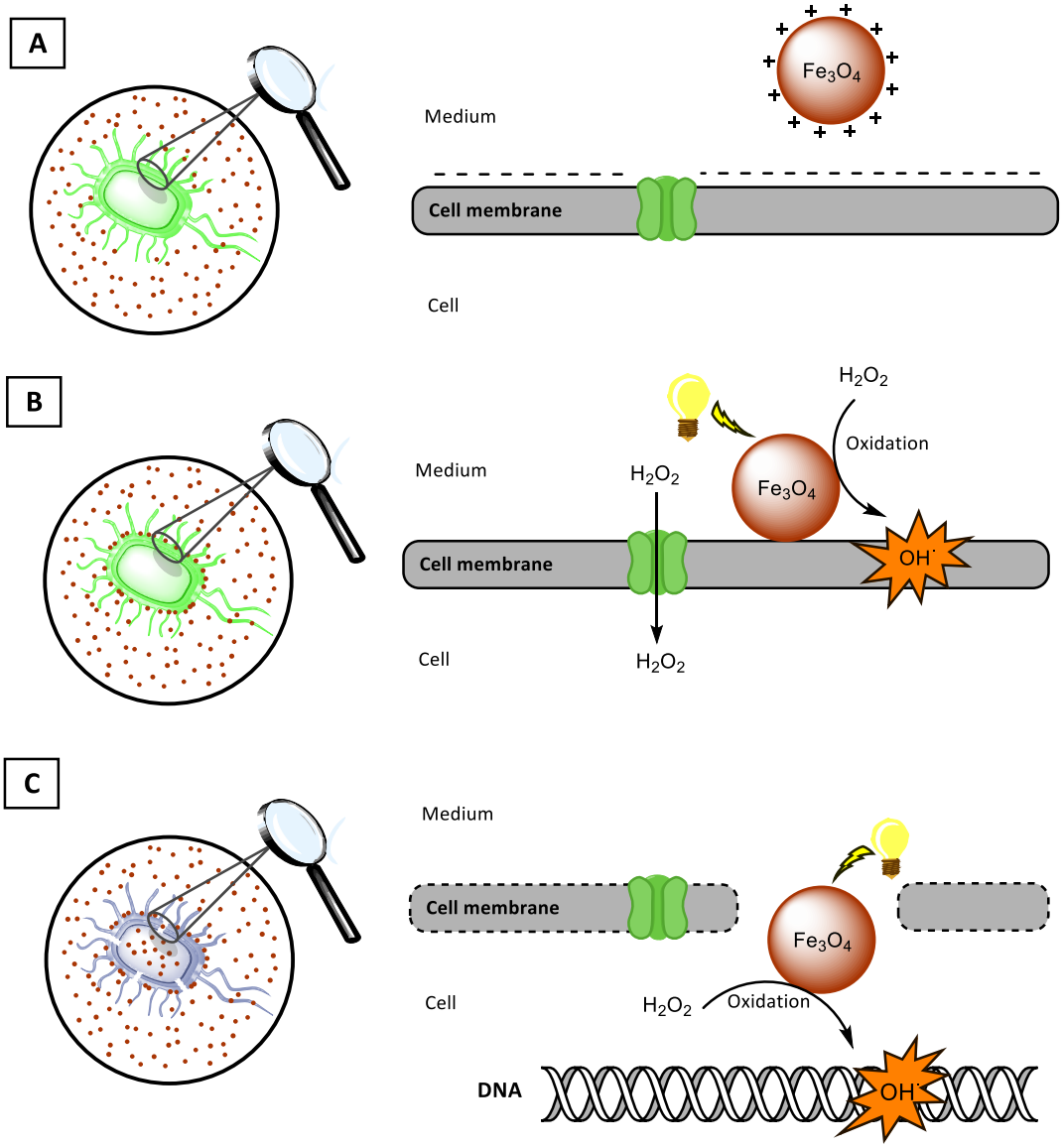


**Figure 1.** Mechanisms of inactivation of bacteria in the photo-Fenton process using magnetite-based nanoparticles.

The application of the Fenton and photo-Fenton processes for the inactivation of *E. coli* or other bacteria has been investigated in several reports, both in free doped catalysts (Liu et al., 2018a) or supported on alginate beads (Barreca et al., 2015), structured silica surfaces (Moncayo-Lasso et al., 2008), membranes or ion exchange resins (Ramírez et al., 2010). The influence of reaction parameters such as catalyst loading, pH conditions, hydrogen peroxide ($H_2O_2$) concentration (Giannakis et al., 2018), light source in the UV-Vis spectrum (Thakur et al., 2020), or sunlight on homogeneous photo-Fenton processes (García-Fernández et al., 2019) has been investigated. The application of electrical discharges to increase the generation of ROS has also been considered, analysing the influence of intensity on the inactivation of microorganisms (Kourdali et al., 2018). From these works, it is possible to identify the main process variables in first-order kinetic models (Ortega-Gómez et al., 2014; Rodríguez-Chueca et al., 2015; Thakur et al., 2020; Zeng et al., 2020), however, the possibility of reusing the catalysts efficiently and with a view to their development on a real scale has not been addressed.

This work proposes to take a step forward in improving the separation of nanocatalysts, focusing the study on the performance of nanostructured magnetic catalysts in experiments under white light of light-emitting diode (LED) and ultraviolet A (UVA) light. The production spectrum of nanoparticles ranges from magnetite-based nanoparticles, in which their surface charge is modified by means of different coatings, to their immobilization on mesoporous silica to improve their stability and increase their specific surface area. Key operational conditions from the point of view of industrial application, such as medium acidity/alkalinity, catalyst loading, hydrogen peroxide concentration and reuse performance should be considered in relation to their influence on the inactivation of total bacterial load present in the secondary effluent of a wastewater treatment plant.

## Materials and methods

### *Chemicals*

Iron (III) chloride hexahydrate ($FeCl_3 \cdot 6H_2O$, 97 wt.%), hydrochloric acid (HCl, 37 wt.%), polyethyleneimine (PEI, 25 kDa), polyacrylic acid (PAA, 2 kDa), the copolymer Triblock Pluronic P123 ($PEO_{20}$-$PPO_{70}$-$PEO_{20}$) and hydrogen peroxide ($H_2O_2$, 30 wt.%) were purchased from Sigma-Aldrich (St. Louis, MI, US). Orthophosphoric acid ($H_3PO_4$, 85 wt.%), ammonium hydroxide ($NH_4OH$, 28 wt.%), iron (II) sulfate heptahydrate ($FeSO_4 \cdot 7H_2O$, 99 wt.%) and tetramethylammonium hydroxide (TMAOH, ≈10 wt.%) were supplied by Fluka (Buchs, ZU, CH); acetone ($CH_3COCH_3$, ≥99 wt.%) and ethanol ($CH_3CH_2OH$, 99 wt.%) by Scharlau (Sentmenat, CT, ES).

### *Synthesis of magnetic nanoparticles and nanocomposites*

The different synthesis routes of magnetic nanoparticles start with the production of sterically stabilized magnetite ($Fe_3O_4$-TMAOH). For this synthesis, $FeSO_4$ and $FeCl_3$ with a molar ratio of 1.5 ($Fe^{3+}/Fe^{2+}$) were dissolved in 100 mL of Milli-Q water containing HCl (0.01 M). Then, the mixture was heated to 60°C in a 250 mL round-bottom flask and 30 mL of $NH_4OH$ (28 wt.%) were added to promote the formation of black magnetite nanoparticles. The nanoparticles were washed three times with water and then the pH was set up at 10 by adding a TMAOH solution (10 wt.%), in order to obtain electrostatically stabilized nanoparticles. Sterically stabilized nanoparticles were obtained by adding different polymers to the reaction. Two different systems were produced: polyacrylic acid ($Fe_3O_4$@PAA) and polyethyleneimine ($Fe_3O_4$@PEI) coated magnetic nanoparticles (Feijoo et al., 2017).

The preparation of the mesostructured silica (SBA-15) was based on the Colilla method (Colilla et al., 2007), using the triblock copolymer Pluronic P123, TEOS and $HCl/HPO_3$. After synthesis, the polymer was dried and washed with organic solvents to remove the remaining chemicals. The synthesis of magnetic nanocomposites, $Fe_3O_4$@PEI/SBA15 and $Fe_3O_4$@PAA/SBA15, is performed by incorporating the SBA-15 matrix into the flask containing the medium used to prepare the sterically stabilized magnetite. After that, the temperature was increased to 60°C and ammonia and PEI or PAA were added to the mixture. The reaction took place for 1 h, and the precipitate formed was acidified to pH 4 with HCl (9 wt.%), and then magnetically separated. Finally, the nanocomposites were washed several times with Milli-Q water and ethanol, and dried for 12 h at 60°C (Osorio et al., 2016).

The structural characterization of the materials was performed by X-ray diffraction (XRD) on powder samples with a Philips PW1710 diffractometer (Cu K$\alpha$ radiation source, $\lambda$ = 1.54186 Å).

The measurements were collected in the 2θ range between 15 and 80°, with steps of 0.020° and 5 s per step. The structure of the mesoporous matrix was analyzed by low-angle XRD in a PANalytical X'Pert Powder Empyrean diffractometer, in a 2θ range between 0.25 and 6°, and a step size of 0.020° (25 s per step). The iron content of the magnetite nanoparticles was obtained from the solid residue of the thermogravimetric curve. The measurements were carried out with a Perkin Elmer TGA7 thermobalance, using $N_2$(g) as purge gas and a scanning rate of 10°C/min. The iron content of the nanocomposites was determined by inductively coupled plasma optical emission spectroscopy (ICP-OES) using a Perkin-Elmer Optima 3300 DV equipped with an autosampler Perkin-Elmer AS91 (Waltham, MA, USA). The samples were directly measured without solid filtration or digestion. Morphological characterization was carried out by scanning electron microscopy, using a Zeiss FE-SEM Ultra Plus microscope (Zeiss, Oberkochen, BW, DE), and transmission electron microscopy, using a JEM-1011 TEM microscope (JEOL, Tokio, 13-JP). The zeta potential of the nanoparticles and nanocomposites was measured with a Malvern Zetasizer Nano ZS (Malvern, Almelo, OV, NL) equipment using the Phase Analysis Light Scattering (PALS) technique. Total pore volume and specific surface area were estimated from $N_2$ adsorption–desorption isotherms obtained using a Quantachrome Autosorb IQ2 instrument.

***Characterization of the municipal WWTP effluent***

The output flow of a secondary clarifier of a WWTP located on Calo–Milladoiro (A Coruña, Spain) was collected twice a week during May – June 2019 to be immediately checked for the presence of pathogens. This plant was designed for a capacity of 9,000 equivalent inhabitants and the water is treated applying primary treatment for the removal of fats and suspended solids; and secondary treatment in an aerobic reactor. The average physicochemical and microbiological characterization of these flow is shown in Table S1.

The TOC content was determined using a Shimadzu TOC 5000 analyzer (Kyoto, JP) and a Metrohom 861 Advanced Compact IC (Herisau, AR, CH) was used to analyze the ion content of samples. Moreover, PetriFilm™ (3M, St. Paul, MN, US) cell culture trays were used to determine the concentration of *E. coli* and total coliforms. All experiments were conducted under aseptic conditions, to rule out the potential of microbial degradation.

***Experimental conditions***

The photocatalysis experiments were performed in 30 mL Erlenmeyer flasks under UVA irradiation (365 nm wavelength UVP PenRay® model 11SC-1L, Analytic Jena, DE) or white light (energy-saving LED lamp of 20 W and 6000 K, Max Lighting, ShenShan, SD, CN). The first step of the experimental procedure involves the adsorption of the microorganisms on the surface of the catalyst by means of electrostatic interactions. The incubation of the wastewater and the nanocatalyst was carried out under dark conditions for 15 min. In the second step, $H_2O_2$ was added to the mixture after taking the first sample and the light source was switched on. The microbiological activity measured at this point was considered to be the initial concentration of microorganisms in terms of colony forming units (CFU). During the experiment, several samples were taken to obtain concentration values against time in order to determine the kinetic parameters.

Experiments were carried out with different types of catalysts: naked, magnetic nanoparticles coated with PAA and PEI, and magnetic nanoparticles supported on SBA15 and also covered with PAA and PEI. The influence of catalyst concentration (50 – 200 mg $L^{-1}$) and $H_2O_2$ concentration (5 – 20 mg $L^{-1}$) was evaluated. Soluble iron in the samples was monitored as a way to determine

the potential solubilization of magnetic NPs. In addition, the individual effect on the inactivation of pathogens associated with the light source, the concentration of $H_2O_2$ and the loading of nanoparticles, as well as the combination of light and $H_2O_2$ were studied in the control experiments.

***Analysis***

Two replicates were withdrawn at the beginning, during and at the end of the experiment in order to monitor viable cells (total coliforms and Escherichia coli). Aliquots of 2 mL were taken and centrifuged at 4000 rpm for 5 min to precipitate the nanoparticles. After that, sequential dilutions of the supernatant were made, and 1 mL of these solutions was cultured in the cell trays to obtain a final concentration value of up to 300 CFU. The counting of the viable cells that survived the treatment (total coliforms and *Escherichia coli*) was determined by incubating the aliquots for 24 and 48 h at 37°C.

The kinetic parameters of the bacterial population were determined based on a pseudo-first-order model, according to the linearization of bacterial growth (Equation 1):

$$\ln (N_0/N) = k \cdot t, \quad (1)$$

were N and $N_0$ are the measured CFU concentrations at time t and $t_0$, k is the kinetic rate constant and t is the time of the experiment.

## Results and discussion

***Characterization of magnetic nanoparticles and nanocomposites***

All the magnetic nanoparticles and nanocomposites were characterized by X-ray powder diffraction (Figure S1A). The peak positions and their relative intensities indicate that the inverse spinel $Fe_3O_4$, magnetite (JPCDS card No. 19-0629), is the main crystalline phase present in the samples. An extra peak for $Fe_3O_4$@PEI/SBA15 nanoparticles corresponding to α-$Fe_2O_3$ (hematite, JPCDS card No. 33-0664) was observed, probably due to the entering of oxygen in the system during the synthesis (made under reductive atmosphere). However, it was not expected an effect in catalyst performance. The magnetic nanocomposites show the presence of magnetite peaks but with low intensity due to the presence of the disordered silica matrix. A broad band is observed at $2\theta$ = 20-25° in the magnetic nanocomposites, which is related to the short-distance disordered structure of the silica matrix. In addition, these magnetic nanocomposites were measured at low-angles ($2\theta$ = 0.25-6.0°) and long-range order was revealed, especially for the sample $Fe_3O_4$@PAA/SBA-15 (Figure S1B). The diffraction peak at *ca.* 0.7º $2\theta$ corresponds to the (100) plane, characteristic of the 2D hexagonal structure (space group *P6m*) of the SBA-15 precursor matrix (Colilla et al., 2007). The absence of this diffraction peak in the $Fe_3O_4$@PEI/SBA-15 sample can be related to a partial alteration of the long-order structure for high magnetite content or to a smaller size of the mesoscale crystalline domains (Vargas-Osorio et al., 2017).

Bare and polymer-coated magnetite nanoparticles have quasi-spherical morphologies and tend to form small aggregates, as depicted in the TEM micrographs (Figures S2.A and S2.B). The average particle size of these nanoparticles is in the range of 8-10 nm: the electrostatically-stabilized bare magnetite nanoparticles, $Fe_3O_4$-TMAOH, has $\langle D_{TEM} \rangle$ = 10.3±2.1 nm (sampling, N = 175); polyacrylic acid coated magnetite nanoparticles, $Fe_3O_4$@PAA, has $\langle D_{TEM} \rangle$ = 7.6±1.7 nm

(sampling, N = 278); and polyethyleneimine coated magnetite nanoparticles, $Fe_3O_4$@PEI, have $<D_{TEM}>$ = 8.5±2.3 nm (sampling, N = 131). As can be observed, the polymer coating promotes the formation of slightly smaller magnetite nanoparticles.

On the other hand, the magnetic nanocomposites formed by the deposition of magnetite nanoparticles onto mesoporous silica matrices showed the 2D hexagonal geometry of the SBA-15 mesoporous silica precursor and small magnetic nanoparticles deposited on the silica surface (Figure S2.C-F). Due to the synthesis method, it is expected that the magnetic nanoparticles could be present both inside and outside the pores.

These magnetic mesoporous nanocomposites were analysed by $N_2$-sorption isotherms. The total pore volumes ($V_p$) were calculated from the $N_2$ adsorption data, and the specific surface area ($S_{BET}$) were obtained from the BET analysis. The nanocomposites showed surface areas of $S_{BET}$ = 157 and 220 $m^2g^{-1}$ and pore volumes of $V_p$ = 0.44 and 0.65 $cm^3g^{-1}$ for $Fe_3O_4$@PEI/SBA-15 and $Fe_3O_4$@PAA/SBA-15, respectively. The iron content of the nanocomposites, as determined by FAAS, was 15 wt% for $Fe_3O_4$@PEI/SBA-15 and 24 wt% for $Fe_3O_4$@PAA/SBA-15.

The coatings of naked $Fe_3O_4$ with PAA and PEI modify their zeta potential, making it slightly negative in the case of PAA and quite positive for PEI. The same trends were observed by other authors with $Fe_3O_4$@citrate nanoparticles (Wang et al., 2009) and SBA15 support (Morales et al., 2019) with PEI. This trend is coincident with the values measured for the polymers without nanoparticles. The characterization values of nanoparticles are shown in Table 1.

**Table 1.** Characterization values of synthesized NPs, coatings and support

| Nanoparticles | pH | ZP (mV) | %Fe w/w | $S_{BET}$ ($m^2$ $g^{-1}$)/ $V_p$ ($cm^3$ $g^{-1}$) | Reference |
|---|---|---|---|---|---|
| Naked $Fe_3O_4$ | 7.0 | -27.0 | 100 | - | (Iyengar et al., 2016) |
| PAA | 7.3 | -41.2 ± 2.8 | 100 | - | |
| PEI | 7.3 | 2.6 ± 1.8 | 100 | - | |
| SBA15 | 7.0 | -35.0 | - | - | (Gómez et al., 2012) |
| $Fe_3O_4$@PAA | 5.8 | -34.8 ± 0.2 | 100 | - | |
| $Fe_3O_4$@PEI | 7.4 | 18.7 ± 0.9 | 100 | - | |
| $Fe_3O_4$@PAA/SBA15 | 7.0 | -30.0 ± 3.2 | 24 | 220/0.65 | |
| $Fe_3O_4$@PEI/SBA15 | - | n.a. | 15 | 157/0.44 | |

n.a.: not allowable

***Control tests***

The control tests were made to prove that the inactivation values are due to the Fenton mechanisms and not due to the medium interactions, as dissolved salts or other compounds present in wastewater. First, the inactivation of the microorganisms in raw samples (without external additions of catalysts, changes on pH and nanoparticles) during the interval of the experiment (30 min) was below the limit of detection (Figure 2). Additionally, the inactivation rates of acidified samples (raw wastewater changed to pH 3) were less than 6%, while cell death increased to 7% when LED light irradiation was applied. On the other hand, control experiments using a few $H_2O_2$ concentrations of 5, 10, 20 and 100 mg $L^{-1}$ were conducted to evaluate the influence of this compound over microorganism inactivation. The toxicity of this chemical on *E. coli* at high concentrations was also studied by other authors (Feuerstein et al., 2006). In this work, concentrations below 10 mg $L^{-1}$ provided a percentage of inactivation lower than 16% for both total coliforms and *E. coli*. A concentration of 20 mg $L^{-1}$ resulted in 40% mortality of microorganisms; however, a value of 100 mg $L^{-1}$ is above the lethal dose and caused the total

inactivation of samples. Finally, the analysis of the influence of $H_2O_2$ in combination with light provided significantly higher inactivation values compared to the control test made only for $H_2O_2$ concentration. The percentages achieved are approximately double those obtained in that case.

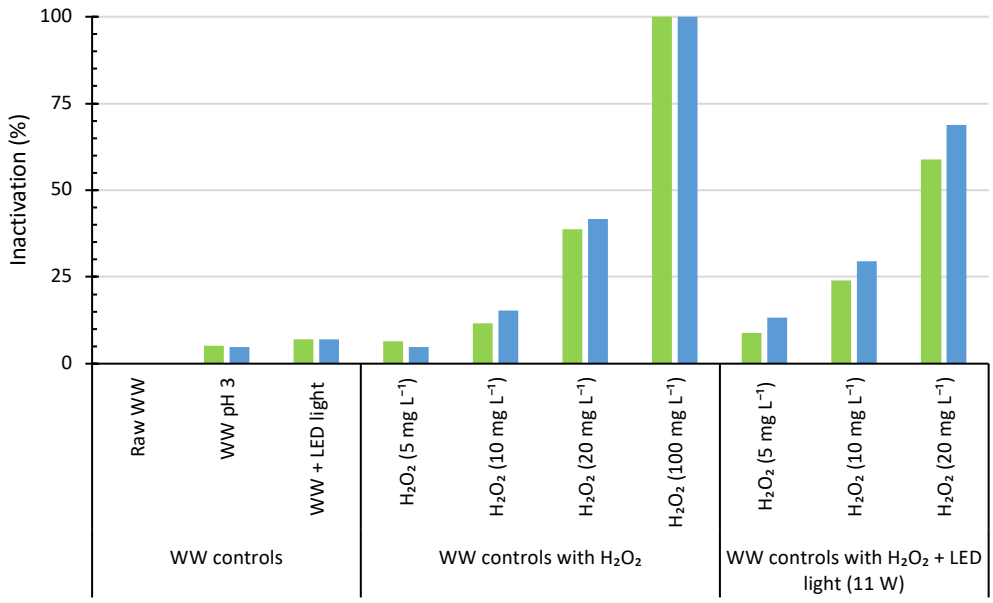


**Figure 2.** Percentages of inactivation by $H_2O_2$ after 30 min for initial microbiological concentrations in the order of 5,000 and 1,000 CFU $mL^{-1}$, respectively, for total coliforms (green) and *E. coli* bacteria (blue).

On the other hand, adsorption controls were performed on free NPs at $Fe_3O_4$ concentrations of 50, 100 and 200 mg $L^{-1}$ putting in contact the catalyst with the samples in raw wastewater, without addition of $H_2O_2$. The supernatant after 30 min was separated, centrifuged and an aliquot was taken for the microorganisms measuring. Thus, the adsorption controls show indirectly the degree of remaining active microorganisms in the effluent after the treatment. Based on the data of the zeta potential (Table 1) it is justified that a similar electrostatic charge results in similar adsorption values.

Moreover, the PEI-coated nanoparticles showed high inactivation rates, which may be due to the fact that the zeta potential value of these nanoparticles was high. A positive value of this electrostatic charge promotes interactions with cell membranes, which have a negative potential, which for *E. coli* bacteria ranges from -40 to -60 mV for pH above 3 (Schwegmann et al., 2010). Also the presence of lipopolysaccharides in the outer membrane increases the negativity of the zeta potential for Gram-negative bacteria, in comparison with Gram-positive ones (i.e. the zeta potential for the Gram-positive *S. aureus* bacteria is about -35 mV, being -44 mV for *E. coli* bacteria under the same conditions) (Halder et al., 2015). In general, the PEI-coated NP immobilized on the SBA15 support increases the adsorption of bacteria on surfaces due to a more positive zeta potential. The results are shown in Figure 3.

Furthermore, for all control tests, the inactivation percentages of *E. coli* followed the same trends as that of total coliforms (both Gram-negative), which shows the similar performance of this process for the inactivation of this type of bacteria. Disparities between the values could be due to the uneven initial concentration used in the experiments. According to the kinetic calculations of the following tests, the inactivation rates were slightly higher for the total coliforms inactivation, showing that the sensitivity of *E. coli* to radical species was lower.

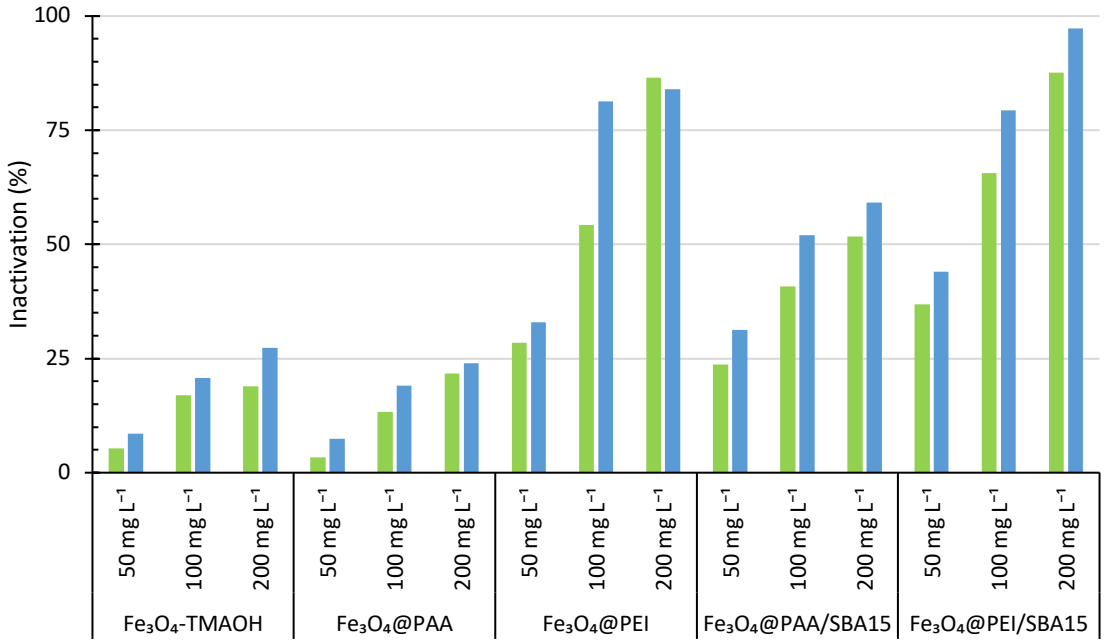


**Figure 3.** Inactivation values for adsorption control experiments after 30 min. Initial microbiological concentrations in the order of 5,000 and 1,000 CFU $mL^{-1}$, respectively, for total coliforms (green) and *E. coli* bacteria (blue). The concentration values are based on magnetite content.

***Screening of NPs***

The influence of Fenton and photo-Fenton nanoparticles on the inactivation of enteric bacteria was evaluated. In parallel, a control with and without light was performed to monitor the contribution of each parameter. In all cases, the initial microbiological concentration of total coliforms was between 5,000 and 6,000 CFU per mL, with *E. coli* strains accounting for about 20%. All these experiments were conducted for a catalyst load of 50 mg $L^{-1}$ based on the magnetite content, equivalent to 12 mg $L^{-1}$ of Fe (II) considering the theoretical composition of pure magnetite. This concentration was selected because the adsorption effects observed in the control experiments were minor, so that the inactivation detected during these tests can be associated mainly with Fenton and photo-Fenton reactions. The experiments were performed at natural pH (around 6.6) and under white light irradiation. In addition, the concentration selected for $H_2O_2$ was 10 mg $L^{-1}$ because it was the highest concentration tested that allowed the catalytic effect to be observed with minimal interactions.

As for the experimental results, the PEI-coated NPs supported by SBA15 showed the best performance (Figure 6.B), achieving complete inactivation of total coliforms after 30 min in the photocatalysis experiments. Under the same conditions, similar trends were shown for the Fenton mechanisms (without light), but in this case, the reaction rate was lower, achieving complete inactivation of total coliforms after 40 min. It should be noted that inactivation due to $H_2O_2$ was in all cases less than 15%. In addition, the $H_2O_2$ experiment combined with light provides a reduction in CFU of less than one order of magnitude. Furthermore, the adsorption of these nanoparticles during the dark period is higher in comparison with the other nanoparticles, reaching 65% of the initial concentration. This performance is similar as shown in the control experiments, and probably caused by the higher electrostatic interaction between these nanoparticles and bacteria caused by the difference in zeta potential.

The results presented by non-supported but PEI-coated NPs (Figure 4.A) highlight the importance of immobilization (Figure 4.B) when assessing the interaction of nanoparticles with bacteria, since under the same conditions, neither photo-Fenton nor Fenton reactions achieved complete inactivation was achieved after 40 min. In this case, the remaining concentration of CFU was 62 and 8 CFU $mL^{-1}$ for the Fenton and photo-Fenton processes, respectively. On the other hand, the performance of both free (Figure 4.C) and SBA15-supported PAA nanoparticles (Figure 4.D) were worse than those of PEI-coated. Similarly, immobilization on mesoporous silica increases the efficiency of the catalyst compared to free ones. In addition, there is a significant contribution of the light that allows the bacterial concentration to be reduced by an order of magnitude lower than that obtained for the Fenton process (without light).

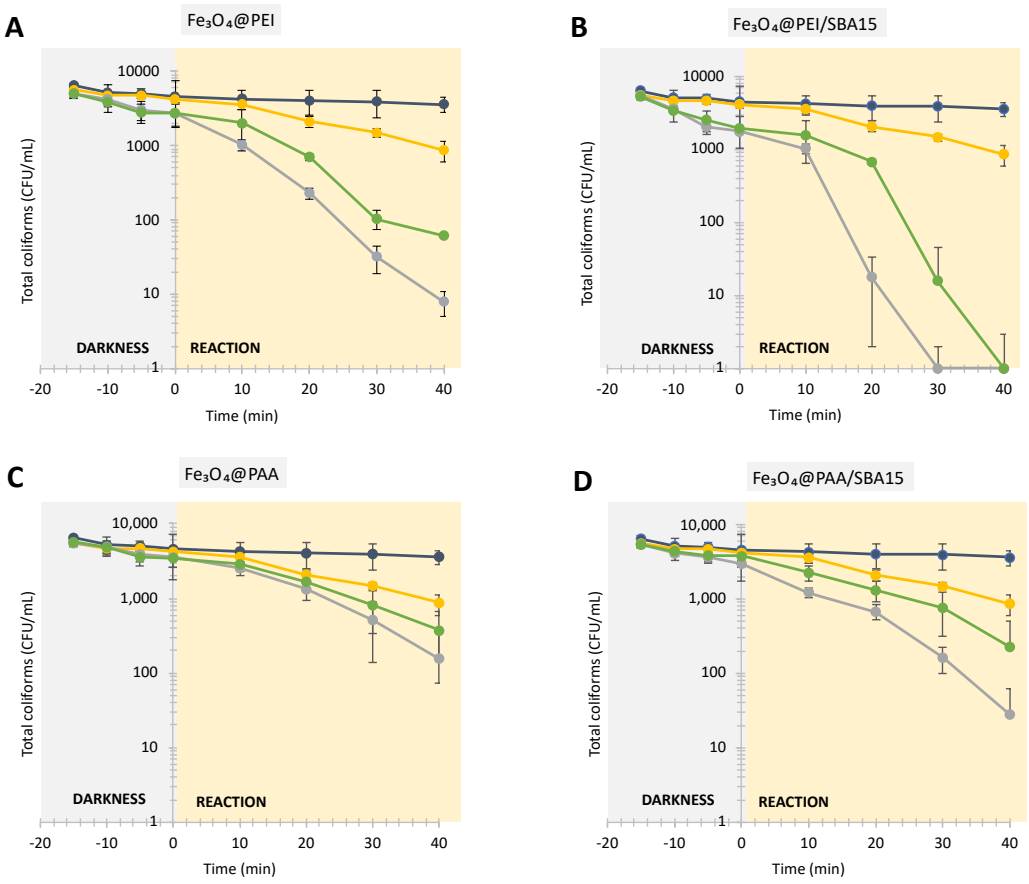


**Figure 4.** Inactivation of total coliforms by Fenton (green) and photo-Fenton (grey) processes under visible light using different types of nanoparticles with concentrations of $Fe_3O_4$ (50 mg $L^{-1}$) and $H_2O_2$ (10 mg $L^{-1}$) at pH of 6.6. Control experiments: inactivation due to light (no $H_2O_2$ or NPs, blue) and light and $H_2O_2$ (no NPs, yellow).

The same conditions (50 mg $L^{-1}$ of catalyst, 10 mg $L^{-1}$ of $H_2O_2$ and natural pH) were used for the study of *E. coli* inactivation, achieving similar inactivation results. In this case, the initial microbiological concentration of microorganisms is around 1000 CFU $mL^{-1}$. The $Fe_3O_4$@PEI/SBA15 NPs (Figure S3.A) showed the best results in terms of inactivation potential and time of incubation, but in this case, the $Fe_3O_4$@PEI NPs (Figure S3.C) reach the null value of *E. coli* CFU under visible light after 40 min. These results were better than those obtained for total coliforms, even considering that the initial concentration of CFU for this case was lower. The performance of PAA-coated nanoparticles (Figure S3.B) was also better, achieving the total inactivation of microorganism after 40 min and under white light. On the other hand, the $Fe_3O_4$@PAA NPs (Figure S3.D) reduces the CFU concentration around two orders of magnitude

for photo-Fenton and one for Fenton reactions, improving the previous findings. These trends are consistent with the results observed in control tests, which show that the sensitivity of *E. coli* against radical attack is higher than the average shown by total coliforms.

In relation to the reuse of water for agricultural purposes, Spanish regulations stipulate that the concentration of *E. coli* after treatment must be below 1 CFU $mL^{-1}$ , being more restrictive than the WHO recommendations, which recommend a concentration of up to 100 CFU $mL^{-1}$ (World Health Organization, 2006). In both regulation frameworks, Fenton and photo-Fenton treatments allow these values to be achieved. Other authors analyzed heterogeneous photo-Fenton processes with supported catalyst but not with nanostructured materials (Moncayo-Lasso et al., 2008), obtaining slower reaction kinetics than those obtained in this work. In the light of the results obtained, an optimization of the conditions for $Fe_3O_4$@PEI/SBA15 NP was conducted, considering that both Fenton and photo-Fenton reactions were obtained with the best results using these NPs. The following steps involve the study of the influence of pH, light source and the optimal concentration of catalyst and $H_2O_2$.

***Optimization of pH***

The selection of the pH has a significant influence on the reaction rates and is a determining factor for the industrial application of these processes. The use of magnetite instead of iron salts as a source of iron allows working in a wide pH window, avoiding the precipitation that occurs in homogeneous Fenton processes without the use of stabilizing agents. The Fenton reaction mechanisms have an optimum pH around 3 (Fenton, 1894), but radical formation also occurs under higher pH conditions, but at lower rates. The performance of the system was evaluated at pH values of 3, 5 and 8, and compared with the natural pH of 6.6.

In the experiments carried out on the inactivation of total coliforms, using the same concentration of catalyst and dose of $H_2O_2$ as in the previous experiments, better results were obtained under acidic conditions, both at pH 3 and pH 5, mainly due to the inactivation caused by the acidic medium and not by photocatalytic degradation, as seen in the control test (data not shown). In the case of pH 3, the inactivation caused by the medium reaches 67%, compared to neutral pH values, where the inactivation was up to 15%. These results followed the trends described by other works (Liu et al., 2018b; Ortega-Gómez et al., 2014). However, the inactivation values do not differ significantly from those obtained for the base case. Control experiments conducted at pH 3 revealed that $H_2O_2$ and light had little effect on the inactivation of the microorganisms. Instead of using a medium at pH 5, the concentration of CFU drops by about an order of magnitude after the experiment, showing that the formation of radicals is due to nanoparticles but also to the breakdown of $H_2O_2$. Experiments performed at pH 8 provided significantly lower inactivation rates than the base case, failing to achieve complete inactivation of total coliforms after 40 min for both Fenton and photo-Fenton reactions.

The results of *E. coli* inactivation were more conclusive, reaching zero concentration for this microorganism after 20 min at pH 3 and for the photo-Fenton reaction. Under the same conditions, the Fenton reaction reached the same value after 30 min. The performance of the nanoparticles at pH 5 is similar, but in this case the inactivation is complete after 30 min for both Fenton and photo-Fenton mechanisms. The lower rates shown for these nanoparticles against total coliforms at pH 8 are similar in the case of *E. coli* inactivation. The kinetic parameters obtained for these experiments are shown in Table 2.

**Table 2**. Kinetic parameters and time needed to achieve a log-3 inactivation obtained considering a pseudo-first order reaction under LED light for pH values from 3 to 8 using $Fe_3O_4$@PEI/SBA15 as catalyst ($[Fe_3O_4]$ = 50 mg $L^{-1}$, $[H_2O_2]$ = 10 mg $L^{-1}$).

| Microorganisms | pH | Fenton | | | | Photo-Fenton | | | |
|---|---|---|---|---|---|---|---|---|---|
| | | k ($h^{-1}$) | σ ($h^{-1}$) | $R^2$ | $t_{3\text{-log}}$ (min) | k ($h^{-1}$) | σ ($h^{-1}$) | $R^2$ | $t_{3\text{-log}}$ (min) |
| Total coliforms | 3.0 | 11.96 | 0.80 | 0.98 | 35 | 13.96 | 1.39 | 0.96 | 30 |
| | 5.0 | 10.72 | 1.28 | 0.95 | 39 | 12.90 | 1.30 | 0.96 | 32 |
| | 6.6 | 9.42 | 1.53 | 0.90 | 44 | 12.40 | 1.20 | 0.96 | 33 |
| | 8.0 | 2.10 | 0.37 | 0.89 | 197 | 3.51 | 0.49 | 0.93 | 118 |
| *E. coli* | 3.0 | 9.71 | 0.72 | 0.98 | 43 | 11.51 | 1.58 | 0.93 | 36 |
| | 5.0 | 9.32 | 0.80 | 0.97 | 44 | 10.33 | 0.98 | 0.97 | 40 |
| | 6.6 | 7.77 | 0.58 | 0.98 | 53 | 8.88 | 0.64 | 0.98 | 47 |
| | 8.0 | 1.17 | 0.30 | 0.80 | 353 | 2.32 | 0.22 | 0.96 | 179 |

The kinetic constants obtained were similar to those reported by other authors in the inactivation of *E. coli* using homogeneous catalysis applying solar irradiation (García-Fernández et al., 2019; Ortega-Gómez et al., 2014). The time required to achieve a log-3 reduction in the best case was about 30 min, achieved in the experiments carried out in the pH range of 3.0 to 6.6. Furthermore, the differences between Fenton and photo-Fenton in terms of kinetic constants were minor (10-20%) with values of $R^2$ above 0.9. The kinetic parameters obtained for the experiments performed at pH 8 are subject to more errors due to the lower reaction rates. Since the experiments were performed for 40 min, the values of the time required for a 3 $\log_{10}$ inactivation above this period were theoretically calculated from the kinetic adjustments.

The similar performance of these catalysts of pH 3 to 6.6 showed that the influence of this variable was not significant in this interval, which offers a clear advantage for their development on a real scale, reducing the costs associated with the consumption of chemicals to adjust the pH and decreasing the impact of the treatment.

***Effect of light source: UVA and white light***

The influence of the light source on the photo-Fenton process occurs because the energy of the photon depends on the wavelength, with lower wavelengths (such as UVA) being more energetic than higher ones (i.e. visible light). Experiments irradiated by white light and UVA light were compared using the optimal concentrations. Under the same conditions, the differences in inactivation between the cases were caused by the change in light. The initial concentrations for total coliforms and *E. coli* were 5000 and 1000 CFU $mL^{-1}$ respectively.

In the experiments monitoring total coliforms, there was an increase in the photo-Fenton reaction, with total inactivation of the microorganisms after 20 minutes under UVA light, compared to the 30 minutes required with samples irradiated with white light. However, the control experiment performed with a combination of hydrogen peroxide and light also showed a drastic reduction of 75% of the total coliforms during the same reaction time. In the case of *E. coli* strains, the lower initial concentration of CFU and the higher susceptibility to radicals compared to the average total coliforms causes the concentration of viable cells to decrease from 1000 to 2 after 10 min. In this case, in control experiments total inactivation was achieved after 30 min. The control experiments, with the exception of UVA light combined with hydrogen peroxide, provide an inactivation value of about 1 $\log_{10}$. Moreover, a 3 $\log_{10}$ reduction of CFU concentration was achieved after 30 min for *E. coli* under UVA light without nanoparticles, only

due to direct photolysis of hydrogen peroxide. Using 25 mg $L^{-1}$ of $H_2O_2$ under combined UVA-visible light, other authors have obtained k-values of 4.2 $h^{-1}$ (Rodríguez-Chueca et al., 2015) similar to those obtained in this work. Moreover, the synergic effect between $H_2O_2$ used in combination with UVA light (Zeng et al., 2020) and visible light (Feuerstein et al., 2006) was also evaluated for the inactivation of bacteria and spores in water. Nevertheless, with catalyst the reaction rate was increased to obtain a kinetic constant around three times higher. The results of these experiments are shown in Figure 5.

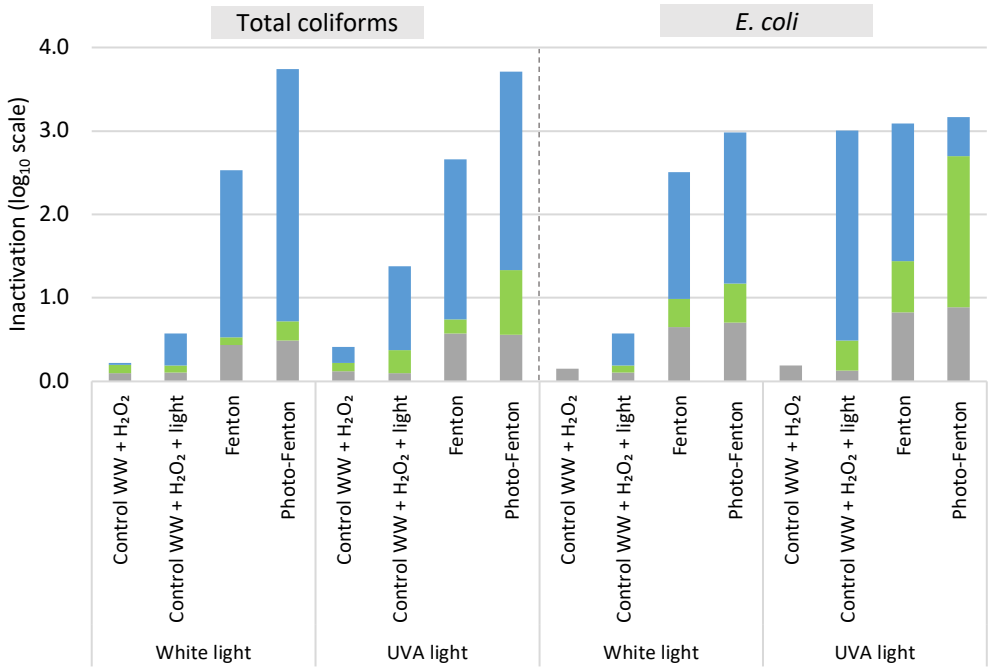


**Figure 5.** Total coliform and *E. coli* inactivation due to adsorption (grey) and Fenton and photo-Fenton processes during 10 min (green) and 30 min (blue) under visible and UVA light using $Fe_3O_4$@PEI/SBA15 as catalyst with concentrations of $Fe_3O_4$ (50 mg $L^{-1}$) and $H_2O_2$ (10 mg $L^{-1}$) at pH of 6.6.

***Addition order effect***

The influence of the addition of hydrogen peroxide and nanoparticles was evaluated. As can be seen in Figure S4, for the inactivation of total coliforms, the influence of hydrogen peroxide in the first step of test, during the equilibrium in darkness, is not significant, achieving practically the same percentages of inactivation without this addition. As for the result, there are no significant differences in the final inactivation in Fenton and photo-Fenton reactions. However, the dosage of catalyst during the process without establishing equilibrium drastically decreases the final inactivation performance, reaching a result of 60 and 500 CFU $mL^{-1}$ for photo-Fenton and Fenton respectively after 40 min of reaction.

The results of *E. coli* inactivation followed the same trends, but in these cases there are less differences between Fenton and photo-Fenton processes, which could be associated with low initial concentrations or high resistance of total coliforms against radicals (data not shown). In other works, the influence of addition has been studied, analyzing the differences in reaction rates when the catalyst was added in steps during the reaction or in a single addition at the beginning. Since in these experiments there were no limitations in the reaction rate caused by

the high concentrations of catalysts, the results were better when iron was added at the beginning (Ortega-Gómez et al., 2014).

***Dissolution of magnetic NPs and evaluation of reuse cycles***

To ensure that the iron present in the medium as unstable solid catalyst or dissolved iron did not affect significatively during the experiments, ICP-OES measurements were made on the treated samples, comparing the results with controls in the absence of NPs. In all cases, both for UVA and white light irradiation, Fenton reaction and adsorption controls, the difference in concentration between the two measurements reaches its maximum value for UVA experiments: 230 ± 8 μg $L^{-1}$. The values obtained in the other cases were below 110 ± 14 μg $L^{-1}$, which shows that in the experiments there could be a contribution due to the homogeneous Fenton process or slight losses of solid catalyst that was not retained by the magnetic field. Considering that the initial concentration of the catalyst was 50 mg $L^{-1}$, the dissolution of iron achieved in the worst case values below 0.5%, which does not represent significant losses.

Finally, the reuse of this catalyst was demonstrated in 10 reuse cycles. To perform the reuse experiments, after the first experiment, the nanoparticles were magnetically separated using a magnet. After this, the supernatant was removed from the flask and fresh wastewater was added in a later step to start another cycle. The results are shown in Figure S5. The performance of the catalyst was maintained throughout the cycles, reaching in most cases inactivation values greater than 3 $\log_{10}$ and 2 $\log_{10}$ for total coliforms and *E. coli* respectively. Taking into account the achieved inactivation percentages, in the case of total coliforms inactivation values of over 99% were achieved in all cases, and without considering the performance in cycle 5, over 99.9%. The inactivation percentage in this cycle was lower compared with the other cycles probably due to a variation in wastewater composition, because this reduction was not maintained in subsequent cycles.

In the case of *E. coli*, because the initial concentration was lower than that used for total coliforms, the sensitivity of the method does not provide the same precision, quantifying at most 99.9% inactivation. In general, similar results were obtained in most cycles. According to the results, the reuse of the catalyst was demonstrated, and the separation of the nanoparticles by means of a magnetic field allows easy recovery without using centrifugation or filtration processes.

## Conclusions

In this work, different magnetite-based nanoparticles with different coatings and supported by mesoporous silica were evaluated for the inactivation of total coliforms and *E. coli* bacteria, analyzing parameters such as pH, hydrogen peroxide concentration. The optimal conditions of the experiments were achieved using the magnetite covered by the PEI and supported by mesoporous silica ($Fe_3O_4$@PEI/SBA15). Compared to non-supported nanoparticles, the deposition of magnetite on SBA15 improves the adsorption of the bacteria on the surface and the inactivation rates obtained were increased. In addition, the PEI coating reduces the negative surface charge of the magnetite, improving the adsorption of bacteria that have a negatively charged cell membrane (i.e. coliforms). The effect of the pH on the inactivation of the bacteria in the range 3 to 6.6 was practically negligible; however, for a pH above this value, the inactivation rates decreased. The high effectiveness of these processes using the natural pH is an advantage over the process application, since it is not necessary to use chemicals to change the acidity of the water, also avoiding the increase of the salt content in the wastewater.

Moreover, the similar performance of the system for both UVA and white light is an advantage over industrial application, because the high energy consumption of UV lights is replaced by light sources that require less energy. Furthermore, the similarity of fluorescent light and solar light to the use of this type of photon source to further realize the sustainability of the process. Finally, the immobilization and coating of the nanoparticles contributed to their stability, as demonstrated in the reuse experiments. Furthermore, the magnetic properties of the nanoparticles allow their separation by the application of magnetic fields, and their effectiveness was demonstrated without a significant decrease in disinfection after ten cycles of reuse. All these characteristics could be interesting for an industrial application of this technology.

**Authors contributions**

**Lucía Fernández:** investigation, writing–review and editing **Jorge González-Rodríguez:** writing—original draft preparation, writing–review and editing **María Gamallo:** investigation, writing–review and editing **Zulema Vargas-Osorio:** resources **Carlos Vázquez-Vázquez:** writing–review and editing, conceptualization and supervision **Yolanda Piñeiro:** resources **José Rivas:** conceptualization and supervision **Gumersindo Feijoo:** conceptualization and supervision **Maria-Teresa Moreira:** writing–review and editing, conceptualization and supervision. All authors have read and agreed to the published version of the manuscript.

**Funding:** This research was supported by two projects granted by Spanish Ministry of Science and Innovation: HP-NANOBIO Project and CLUSTERCAT Project MAT2015-67458-P, and Fundación Ramón Areces, Spain (Project CIVP18A3940). The authors belong to the Galician Competitive Research Groups ED431C-2017/22 and ED431C-2017/29 and CRETUS Institute.

**Acknowledgments:** J.G.-R. thanks the Xunta de Galicia Counseling of Education for his predoctoral fellowship. M.T.M., G.F. and J.G.-R. belong to CRETUS Institute. The authors also thank Xunta de Galicia for the CRETUS (AGRUP2015/02) and AEMAT (ED431E-2018/08) Strategic Partnerships, and the use of RIAIDT-USC analytical facilities. The authors belong to the Galician Competitive Research Groups ED431C-2017/22 and ED431C-2017/29, co-funded by FEDER.
**Conflicts of Interest:** The authors declare no conflict of interest.

# References

Baniamerian, H., Safavi, M., Alvarado-Morales, M., Tsapekos, P., Angelidaki, I., Shokrollahzadeh, S., 2018. Photocatalytic inactivation of Vibrio fischeri using Fe 2 O 3 -TiO 2 -based nanoparticles. Environ. Res. 166, 497–506. https://doi.org/10.1016/j.envres.2018.06.011

Barreca, S., Velez Colmenares, J.J., Pace, A., Orecchio, S., Pulgarin, C., 2015. Escherichia coli inactivation by neutral solar heterogeneous photo-Fenton (HPF) over hybrid iron/montmorillonite/alginate beads. J. Environ. Chem. Eng. 3, 317–324. https://doi.org/10.1016/J.JECE.2014.10.018

Bautista, P., Mohedano, A.F., Casas, J.A., Zazo, J.A., Rodriguez, J.J., 2008. An overview of the application of Fenton oxidation to industrial wastewaters treatment. J. Chem. Technol. Biotechnol. 83, 1323–1338. https://doi.org/10.1002/jctb.1988

Chong, M.N., Jin, B., Chow, C.W.K., Saint, C., 2010. Recent developments in photocatalytic water treatment technology: A review. Water Res. 44, 2997–3027. https://doi.org///doi.org/10.1016/j.watres.2010.02.039

Colilla, M., Balas, F., Manzano, M., Vallet-Regí, M., 2007. Novel method to enlarge the surface area of SBA-15. Chem. Mater. 19, 3099–3101. https://doi.org/10.1021/cm071032p

Davididou, K., Chatzisymeon, E., Perez-Estrada, L., Oller, I., Malato, S., 2019. Photo-Fenton treatment of saccharin in a solar pilot compound parabolic collector: Use of olive mill wastewater as iron chelating agent, preliminary results. J. Hazard. Mater. 372, 137–144. https://doi.org/10.1016/j.jhazmat.2018.03.016

European Union, 1991. Council Directive 91/271/EEC of 21 May 1991 concerning urban waste-water treatment. Europe. https://doi.org/http://eur-lex.europa.eu/legal-content/en/ALL/?uri=CELEX:31991L0271

Feijoo, S., González-García, S., Moldes-Diz, Y., Vazquez-Vazquez, C., Feijoo, G., Moreira, M.T., 2017. Comparative life cycle assessment of different synthesis routes of magnetic nanoparticles. J. Clean. Prod. 143, 528–538. https://doi.org/10.1016/j.jclepro.2016.12.079

Fenton, H.J.H., 1894. LXXIII.—Oxidation of tartaric acid in presence of iron. J. Chem. Soc. Trans. 65, 899–910. https://doi.org/10.1039/CT8946500899

Fernández, L., Gamallo, M., González-Gómez, M.A., Vázquez-Vázquez, C., Rivas, J., Pintado, M., Moreira, M.T., 2019. Insight into antibiotics removal: Exploring the photocatalytic performance of a Fe3O4/ZnO nanocomposite in a novel magnetic sequential batch reactor. J. Environ. Manage. 237, 595–608.

https://doi.org/10.1016/J.JENVMAN.2019.02.089
Ferreiro, C., Villota, N., Lombraña, J.I., Rivero, M.J., 2019. An efficient catalytic process for the treatment of genotoxic aniline wastewater using a new granular activated carbon-supported titanium dioxide composite. J. Clean. Prod. 228, 1282–1295. https://doi.org/10.1016/j.jclepro.2019.04.198
Feuerstein, O., Moreinos, D., Steinberg, D., 2006. Synergic antibacterial effect between visible light and hydrogen peroxide on Streptococcus mutans. J. Antimicrob. Chemother. 57, 872–876. https://doi.org/10.1093/jac/dkl070
García-Fernández, I., Miralles-Cuevas, S., Oller, I., Fernández-Ibáñez, P., Polo-López, M.I., 2019. Inactivation of E. coli and E. faecalis by solar photo-Fenton with EDDS complex at neutral pH in municipal wastewater effluents. J. Hazard. Mater. 372, 85–93. https://doi.org/10.1016/J.JHAZMAT.2018.07.037
Giannakis, S., Le, T.T.M., Entenza, J.M., Pulgarin, C., 2018. Solar photo-Fenton disinfection of 11 antibiotic-resistant bacteria (ARB) and elimination of representative AR genes. Evidence that antibiotic resistance does not imply resistance to oxidative treatment. Water Res. 143, 334–345. https://doi.org/10.1016/j.watres.2018.06.062
Giannakis, S., López, M.I.P., Spuhler, D., Pérez, J.A.S., Ibáñez, P.F., Pulgarin, C., 2016. Solar disinfection is an augmentable, in situ-generated photo-Fenton reaction-Part 2: A review of the applications for drinking water and wastewater disinfection. Appl. Catal. B Environ. 198, 431–446. https://doi.org/10.1016/j.apcatb.2016.06.007
Gómez, J.M., Romero, M.D., Fernández, T.M., Díez, E., 2012. Immobilization of β-glucosidase in fixed bed reactor and evaluation of the enzymatic activity. Bioprocess Biosyst. Eng. 35, 1399–1405. https://doi.org/10.1007/s00449-012-0728-y
González-Rodríguez, J., Fernández, L., Bava, Y.B., Buceta, D., Vázquez-Vázquez, C., López-Quintela, M.A., Feijoo, G., Moreira, M.T., 2020. Enhanced photocatalytic activity of semiconductor nanocomposites doped with ag nanoclusters under UV and visible light. Catalysts 10, 31. https://doi.org/10.3390/catal10010031
Halder, S., Yadav, K.K., Sarkar, R., Mukherjee, S., Saha, P., Haldar, S., Karmakar, S., Sen, T., 2015. Alteration of Zeta potential and membrane permeability in bacteria: a study with cationic agents. Springerplus 4, 1–14. https://doi.org/10.1186/s40064-015-1476-7
Iyengar, S.J., Joy, M., Maity, T., Chakraborty, J., Kotnala, R.K., Ghosh, S., 2016. Colloidal properties of water dispersible magnetite nanoparticles by photon correlation spectroscopy. RSC Adv. 6, 14393–14402. https://doi.org/10.1039/c5ra26488j
Kourdali, S., Badis, A., Boucherit, A., Boudjema, K., Saiba, A., 2018. Electrochemical disinfection of bacterial contamination: Effectiveness and modeling study of E. coli inactivation by electro-Fenton, electro-peroxi-coagulation and electrocoagulation. J. Environ. Manage. 226, 106–119. https://doi.org/10.1016/J.JENVMAN.2018.08.038
Laxma Reddy, P.V., Kavitha, B., Kumar Reddy, P.A., Kim, K.H., 2017. TiO2-based photocatalytic disinfection of microbes in aqueous media: A review. Environ. Res. 154, 296–303. https://doi.org/10.1016/j.envres.2017.01.018
Liu, J., Dong, C., Deng, Y., Ji, J., Bao, S., Chen, C., Shen, B., Zhang, J., Xing, M., 2018a. Molybdenum sulfide Co-catalytic Fenton reaction for rapid and efficient inactivation of Escherichia coli. Water Res. 145, 312–320. https://doi.org/10.1016/J.WATRES.2018.08.039
Liu, J., Dong, C., Deng, Y., Ji, J., Bao, S., Chen, C., Shen, B., Zhang, J., Xing, M., 2018b. Molybdenum sulfide Co-catalytic Fenton reaction for rapid and efficient inactivation of Escherichia coli. Water Res. 145, 312–320. https://doi.org/10.1016/j.watres.2018.08.039
Miralles-Cuevas, S., Oller, I., Pérez, J.A.S., Malato, S., 2014. Removal of pharmaceuticals from MWTP effluent by nanofiltration and solar photo-Fenton using two different iron complexes at neutral pH. Water Res. 64, 23–31. https://doi.org///doi.org/10.1016/j.watres.2014.06.032
Mirzaei, A., Chen, Z., Haghighat, F., Yerushalmi, L., 2017. Removal of pharmaceuticals from water by homo/heterogonous Fenton-type processes – A review. Chemosphere 174, 665–688. https://doi.org/10.1016/j.chemosphere.2017.02.019
Mirzaei, A., Chen, Z., Haghighat, F., Yerushalmi, L., 2016. Removal of pharmaceuticals and endocrine disrupting compounds from water by zinc oxide-based photocatalytic degradation: A review. Sustain. Cities Soc. 27, 407–418. https://doi.org///doi.org/10.1016/j.scs.2016.08.004
Moncayo-Lasso, A., Torres-Palma, R.A., Kiwi, J., Benítez, N., Pulgarin, C., 2008. Bacterial inactivation and organic oxidation via immobilized photo-Fenton reagent on structured silica surfaces. Appl. Catal. B Environ. 84, 577–583. https://doi.org/10.1016/j.apcatb.2008.05.022
Morales, V., Martín, A., Ortiz-Bustos, J., Sanz, R., García-Muñoz, R.A., 2019. Effect of the dual incorporation of fullerene and polyethyleneimine moieties into SBA-15 materials as platforms for drug delivery. J. Mater. Sci. 54, 11635–11653. https://doi.org/10.1007/s10853-019-03708-0
Ortega-Gómez, E., Esteban García, B., Ballesteros Martín, M.M., Fernández Ibáñez, P., Sánchez Pérez, J.A., 2014. Inactivation of natural enteric bacteria in real municipal wastewater by solar photo-Fenton at neutral pH. Water Res. 63, 316–324. https://doi.org/10.1016/j.watres.2014.05.034
Osorio, Z.V., Pineiro, Y., Vazquez, C., Abreu, C.R., Perez, M.A.A., Quintela, M.A.L., Rivas, J., 2016. Magnetic nanocomposites based on mesoporous silica for biomedical applications. Int. J. Nanotechnol. 13, 648. https://doi.org/10.1504/IJNT.2016.079668
Pigeot-Rémy, S., Simonet, F., Errazuriz-Cerda, E., Lazzaroni, J.C., Atlan, D., Guillard, C., 2011. Photocatalysis and

disinfection of water: Identification of potential bacterial targets. Appl. Catal. B Environ. 104, 390–398. https://doi.org/10.1016/j.apcatb.2011.03.001
Purnell, S., Halliday, A., Newman, F., Sinclair, C., Ebdon, J., 2020. Pathogen infection risk to recreational water users, associated with surface waters impacted by de facto and indirect potable reuse activities. Sci. Total Environ. 722, 137799. https://doi.org/10.1016/j.scitotenv.2020.137799
Ramírez, J., Godínez, L.A., Méndez, M., Meas, Y., Rodríguez, F.J., 2010. Heterogeneous photo-electro-Fenton process using different iron supporting materials. J. Appl. Electrochem. 40, 1729–1736. https://doi.org/10.1007/s10800-010-0157-z
Rodríguez-Chueca, J., Ormad, M.P., Mosteo, R., Ovelleiro, J.L., 2015. Kinetic modeling of Escherichia coli and Enterococcus sp. inactivation in wastewater treatment by photo-Fenton and H2O2/UV–vis processes. Chem. Eng. Sci. 138, 730–740. https://doi.org/10.1016/J.CES.2015.08.051
Rodriguez-Narvaez, O.M., Peralta-Hernandez, J.M., Goonetilleke, A., Bandala, E.R., 2017. Treatment technologies for emerging contaminants in water: A review. Chem. Eng. J. https://doi.org/10.1016/j.cej.2017.04.106
Schwegmann, H., Feitz, A.J., Frimmel, F.H., 2010. Influence of the zeta potential on the sorption and toxicity of iron oxide nanoparticles on S. cerevisiae and E. coli. J. Colloid Interface Sci. 347, 43–48. https://doi.org/10.1016/j.jcis.2010.02.028
Sgroi, M., Vagliasindi, F.G.A., Roccaro, P., 2018. Feasibility, sustainability and circular economy concepts in water reuse. Curr. Opin. Environ. Sci. Heal. https://doi.org/10.1016/j.coesh.2018.01.004
Shannon, M.A., Bohn, P.W., Elimelech, M., Georgiadis, J.G., Marĩas, B.J., Mayes, A.M., 2008. Science and technology for water purification in the coming decades. Nature. https://doi.org/10.1038/nature06599
Thakur, I., Örmeci, B., verma, A., 2020. Inactivation of E. coli in water employing Fe-TiO2 composite incorporating in-situ dual process of photocatalysis and photo-Fenton in fixed-mode. J. Water Process Eng. 33, 101085. https://doi.org/10.1016/j.jwpe.2019.101085
US Environmental Protection Agency, 2012. Guidelines for Water Reuse, Development. https://doi.org/EPA16251R-921004
Vargas-Osorio, Z., González-Gómez, M.A., Piñeiro, Y., Vázquez-Vázquez, C., Rodríguez-Abreu, C., López-Quintela, M.A., Rivas, J. Novel synthetic routes of large-pore magnetic mesoporous nanocomposites (SBA-15/Fe3O4) as potential multifunctional theranostic nanodevices. J. Mater. Chem. B 5, 9395-9404. https://doi.org/10.1039/c7tb01963g
Wang, X., Zhou, L., Ma, Y., Li, X., Gu, H., 2009. Control of aggregate size of polyethyleneimine-coated magnetic nanoparticles for magnetofection. Nano Res. 2, 365–372. https://doi.org/10.1007/s12274-009-9035-6
World Health Organization, 2006. WHO guidelines for the safe use of wastewater, excreta and greywater, World Health. World Health Organization. https://doi.org/10.1007/s13398-014-0173-7.2
Zeng, F., Cao, S., Jin, W., Zhou, X., Ding, W., Tu, R., Han, S.-F., Wang, C., Jiang, Q., Huang, H., Ding, F., 2020. Inactivation of chlorine-resistant bacterial spores in drinking water using UV irradiation, UV/Hydrogen peroxide and UV/Peroxymonosulfate: Efficiency and mechanism. J. Clean. Prod. 243, 118666. https://doi.org/10.1016/J.JCLEPRO.2019.118666